Indian Journal of Science and Technology, *Vol 8(16), DOI: 10.17485/ijst/2015/v8i16/58537, July 2015*
ISSN (Print) : 0974-6846
ISSN (Online) : 0974-5645

Modified Speed Sensor-less Grid Connected DFIG based WECS

Subir Datta[1*], J. P. Mishra[2] and A. K. Roy[3]

[1]Department of Electrical Engineering, Mizoram University, Aizawl, Mizoram - 7960 04, India; subirnerist@gmail.com
[2]Department of Electrical Engineering, National Institute of Technology, Silchar - 788 010, India; jpm.nits@gmail.com, anjan_kumarrroy@rediffmail.com
[3]Department of Electrical Engineering, Tripura Institute of Technology, Agartala - 799009, Tripura, India; anjan_kumarrroy@rediffmail.com

Abstract

This paper presents a new Phase Locked Loop (PLL) based slip speed estimator for speed sensor less field oriented vector control operation of variable speed grid connected Wind Energy Conversion System (WECS). Three phase rotor current is used to design a PLL based slip estimator for speed sensor-less vector control operation of rotor side converter. The proposed speed sensor-less grid connected Double Fed Induction Generator (DFIG) based WECS is used for decoupled control of stator active and reactive power to ensure maximizing the power generation at unity power factor under varying wind speed. The speed sensor-less Vector control scheme is also incorporated with an optimal speed tracking controller for maximum energy capture in the rated wind speed range and restrict the mechanical output power to the rated value using pitch angle control when the wind velocity crosses rated limit to prevent overloading and outage of the wind turbine. The proposed method does not require the information of rotor speed or position for speed sensor less DFIG based WECS unlike other published methods. Simulation has been carried out in MATLAB/Simulink environment and results have been analyzed. Results show that the proposed speed sensor-less DFIG system can operate at its optimum energy level for a wide range of wind speed and is capable for satisfactory operation of the variable speed WECS.

Keywords: DFIG, PLL, Slip Speed Estimator, Speed Sensor-Less, WECS

1. Introduction

Now-a-days, Doubly Fed Induction Generator (DFIG) system, comprising of a slip-ring induction generator, a back-to-back AC-DC-AC electronic converter and a common DC-link capacitor has become one of the most popular wind generator systems. The back-to-back AC-DC-AC voltage source converter has two main parts: Grid Side Converter (GSC) to rectify grid voltage and Rotor Side Converter (RSC) to feed controllable voltage to the rotor circuit of DFIG[1]. Power electronics converter processes only the slip power. Therefore it is designed in partial scale, for just about 30% of generator rated power[2]. This causes reduction in converter cost, injection of less harmonics to the grid, improves overall energy conversion efficiency[3–6] and further, there exists scope for independent control of active and reactive powers. The DFIG can act as a variable speed generator in stand-alone and grid connected applications. Speed sensor–less DFIG based vector control is desirable in both grid and stand-alone connected wind energy conversion system as shaft speed sensors has some demerits in terms of robustness, maintenance, cost and cable connection between the speed sensors and controllers and the most significant failure modes of the system is encoder failure. Several open loop speed sensor methods have been published by many researchers for DFIG system. In [7–10], the position of rotor is obtained by comparing estimated and measured rotor currents and that rotor position is differentiated to obtain rotor speed. However, the methodology and observer modeling are not presented in [7–10]

*Author for correspondence

for the whole open-loop base speed sensor less system. In [11,12], the machine equations are used to derive the magnetizing current for an observer model, but methodology for design and modeling of observer system was not discussed. In [13,14], speed sensor-less methods are proposed based on rotor flux which is calculated by integration of the rotor back emf, although the rotor flux cannot be accurately estimated by integrating rotor back emf due to low frequencies in the rotor. In [15–17], observer models based on adaptive system are proposed for speed sensor-less control of squirrel cage induction machines. In[18], rotor flux, stator flux, stator current and rotor current based Model Reference Adaptive System (MRAS) observers are proposed and their advantages and disadvantages for stand-alone and grid connected mode operation are discussed. In [19], a speed sensor less reactive power based MRAS control scheme was proposed where information of rotor speed or position is not required for field orientation of the rotor variables. But this method cannot estimate the value of slip speed (ω_{slip}) correctly as this method is more sensitive on machine parameters and a no line magnetizing inductance (L_m) estimator is required to estimate the value of ω_{slip}. Hence, the method is quite complex and cannot estimate slip speed correctly. In this paper a new speed sensor-less grid connected control scheme is presented and this algorithm does not require the rotor position or speed information for the stator field orientation of the rotor variables. The slip speed estimation is still necessary for back e.m.f. compensation in the rotor controllers. For this purpose a three phase rotor current (I_{abcr}) based PLL is proposed. Initially, a circuitry simulation model of a 1.5MW variable wind turbine with a DFIG is developed in MATLAB/Simulink. The aerodynamic model of the wind turbine along with the electrical model and detail control schemes of the DFIG based wind turbine is described then.

2. Modeling and Control of the DFIG Wind Turbine

Figure 1 shows the basic structure of a DFIG Wind Turbine system. DFIG is a wound rotor Induction Machine. Its stator terminals are directly connected to the grid, while the rotor terminals are connected to the same grid, but via a PWM back-to-back converter which consists of Rotor Side Converter (RSC) and a Grid Side Converter (GSC)[20]. The wind turbine is mechanically coupled to the shaft of DFIG's rotor via gear.

2.1 Modeling of the Wind Turbine

The mechanical power P_m captured by the turbine from the wind for a given wind speed (V_w) is computed by the following expression[21,22,27]:

$$P_m = \frac{\partial}{\partial t}(E_w) * C_p = \frac{1}{2}\rho V_w^3 C_p \quad (1)$$

Equation (1) shows that the power coefficient, Cp, depends on the speed ratio 'λ' and the pitch angle 'β' of the rotor blades. The tip speed ratio is defined as the ratio between the speed of tip of the blade and the wind speed as follows:

$$\lambda = \frac{R * \omega_r}{V_W} \quad (2)$$

The pitch angle 'β', for high power wind turbines, is the output variable of pitch control system. Value of 'β' is adjusted depending upon wind speed, length of the blades and the tip speed. Taking both (i.e. tip speed ratio and pitch angle) parameters into account, an approximated Cp curve is given by equation (3) as in[21, 23, 27]:

$$C_p = 0.5176\left(\frac{116}{\lambda_i} - 0.4\beta - 5\right)e^{\frac{-21}{\lambda_i}} + 0.0068\lambda \quad (3)$$

where,

$$\lambda_i = \frac{1}{\frac{1}{\lambda + 0.08\lambda} - \frac{0.035}{\beta^3 + 1}}$$

Since Cp= f (λ, β), the plot of C^p Vs λ at various values of β is shown in Figure 2. For β equal to zero the maximum Cp value is bounded according to Betz's limit. The corresponding torque curve, depending on the rotor turbine speed, is presented in Figure 3 to illustrate the correspondence between the wind turbine torque and the rotor speed. According to equation (4), the electrical power generated comes out from the product of the mechanical torque and the rotational speed of the shaft.

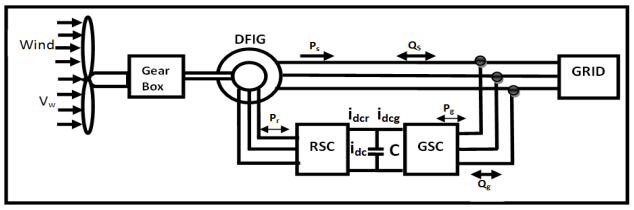

Figure 1. Structure of the DFIG based WECS[29].

$$P = T_m \omega_m \quad (4)$$

In Figure 4 shows the amount of electrical power developed at different rotor speeds (produced at different wind speeds).

2.2 Maximum Power Point Tracking (MPPT)

The objective of the MPPT mode of operation is to extract maximum possible power at different wind speeds, in low to medium range, by following the maximum value of the wind power coefficient (C_{p_max}), as depicted in Figure 4. From the plot shown in Figure 2, it can be stated that, for $\beta=0^0$, $\lambda_{opt}=8.1$ and $C_{p\_max} = 0.48$. Now the rotor mechanical torque that drives the DFIG is[21]:

$$T_t = \frac{P_m}{\omega_t} \quad (5)$$

Now from equations (1) and (5), we get

$$T_t = \frac{1}{2\omega_t}\rho A V_\omega^3 C_p = \frac{R}{2\lambda}\rho V_\omega^3 C_I \quad (6)$$

If C_p is maintained constant, equal to C_{p_max} under MPPT mode, the expression for the maximum extracted power, from equation (1), can be written as

$$P_{max} = K^* V_\omega^3 \quad (7)$$

Where, $K = \frac{1}{2}\rho A C_{p\_max}$ = Constant

The plot of the maximum extracted power that can be derived at different rotor speeds is shown in Figure 4. The mechanism for MPPT of the wind turbine is coded on MATLAB/Simulink Embedded-MALTAB function environment and is explained in the flow chart shown in Figure 5.

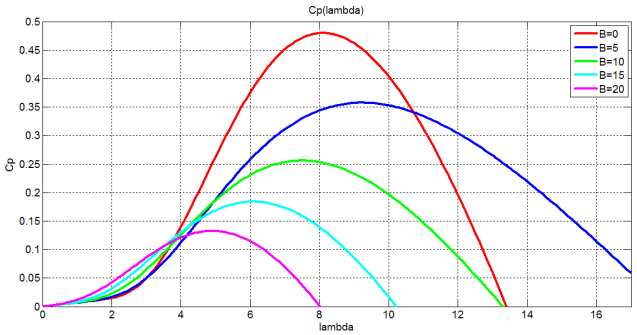

Figure 2. Cp Vs λ for different β.

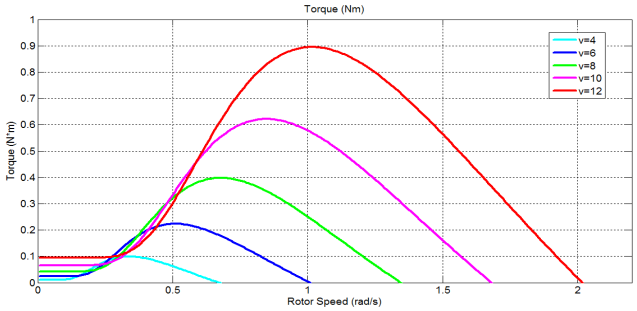

Figure 3. Wind Turbine Torque Vs Speed Characteristic.

2.3 Pitch Angle Controller

When the wind velocity increases beyond the rated value, the electromagnetic torque and hence rotor speed becomes too high to control. To restrict rotor speed from becoming too high, the extracted power from incoming wind is restricted to its rated value by reducing the power coefficient (C_p value) using pitch angle control, as shown in Figure 2. The mechanism for blade pitch angle control of the wind turbine is coded on MATLAB/Simulink S-function environment and explained in the flowchart shown in Figure 6.

2.4 Modeling of the DFIG

A DFIG has several advantages over conventional Induction Machine in wind power applications[24]. The operating principle of a DFIM can be analyzed using the classical theory of rotating fields and the well-known d-q model, involving both three-to-two and two-to-three phase axes transformations[25]. In order to deal with the machine dynamics, in the most realistic possible way, both stator and rotor variables are referred to their corresponding natural reference frames. In other words, the stator side current and voltage

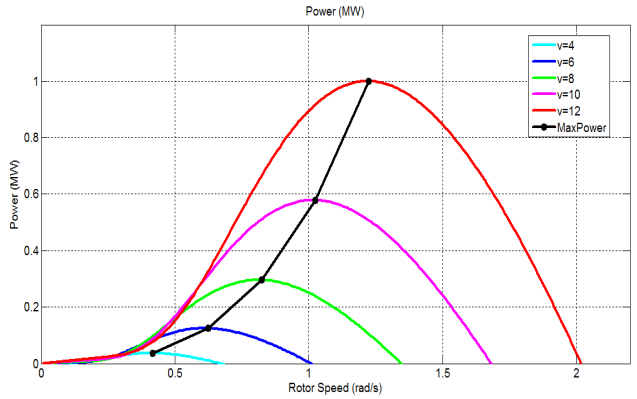

Figure 4. Wind Turbine Developed Power Vs Speed Characteristic.

components are referred to a stationary reference frame, while the rotor side current and voltage components are referred to a reference frame rotating at rotor speed (in electrical rad/sec).

The equations for voltages and fluxes, in the arbitrary d-q reference frames, are[25]:

$$\left.\begin{aligned} V_{sd} &= R_s i_{sd} + \frac{d}{dt}\psi_{sd} - \omega\psi_{sq} \\ V_{sq} &= R_s i_{sq} + \frac{d}{dt}\psi_{sq} + \omega\psi_{sd} \\ V_{rd} &= R_s i_{sd} + \frac{d}{dt}\psi_{rd} - (\omega - \omega_r)\psi_{rq} \\ V_{rq} &= R_s i_{sq} + \frac{d}{dt}\psi_{rq} + (\omega - \omega_r)\psi_{rd} \end{aligned}\right\} \quad (8)$$

The flux linkages are given by:

$$\left.\begin{aligned} \psi_{sd} &= L_s i_{sd} + L_m i_{rd} \\ \psi_{sq} &= L_s i_{sq} + L_m i_{rq} \\ \psi_{rd} &= L_r i_{rd} + L_m i_{sd} \\ \psi_{rq} &= L_r i_{rq} + L_m i_{sq} \end{aligned}\right\} \quad (9)$$

The electromagnetic torque developed by the DFIG can be expressed as:

$$T_{em} = \frac{3}{2} * \frac{P}{2} * \left(\psi_{sd}^{*} i_{sq} - \psi_{sq}^{*} i_{sd}\right) \quad (10)$$

The active and reactive stator power can be expressed as[28]:

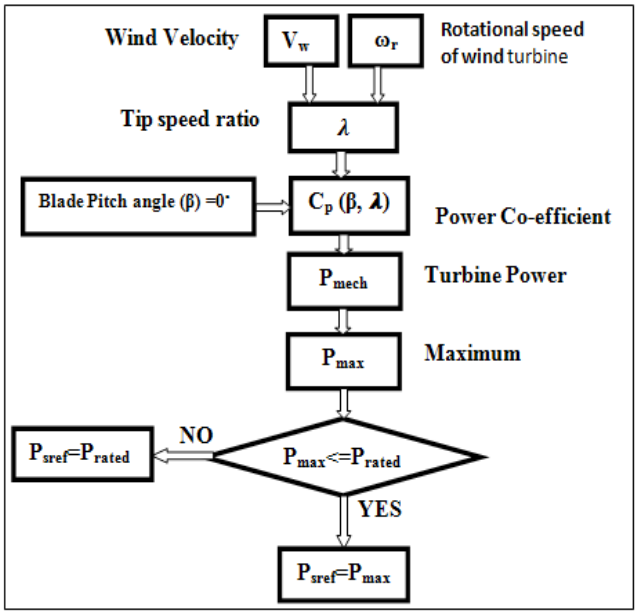

Figure 5. Flow Chart for Maximum power point tracking.

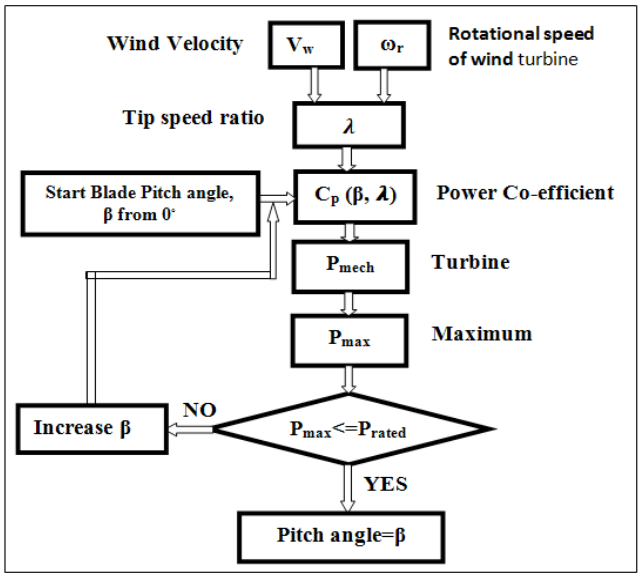

Figure 6. Flowchart for Pitch Angle Controller.

$$P_s = \frac{3}{2}\left(V_{sd} i_{sd} + V_{sq} i_{sq}\right) \quad (11)$$

$$Q_s = \frac{3}{2}\left(V_{sq} i_{sd} - V_{sd} i_{sq}\right) \quad (12)$$

3. Vector Control of the DFIG Wind Turbine

The Vector control of wind turbine coupled DFIG is achieved by controlling RSC and GSC. RSC is controlled for getting independent control of active power Ps and reactive power Q_s of the stator. GSC is controlled for maintaining constant dc-link voltage V_{dc} and to regulate exchange of reactive power Q_g between GSC and grid[26].

3.1 Vector-control Scheme of GSC

Grid-voltage-oriented vector control approach is used for GSC to achieve independent control of active power between grid and DC link (using d-axis current, for maintaining constant dc-link voltage V_{dc}) and reactive power between the grid and grid-side converter (using q-axis current). Figure 7 shows the schematic of the grid-side PWM voltage source converter. The voltage balance across the inductor

$$\begin{bmatrix} V_{ga} \\ V_{gb} \\ V_{gc} \end{bmatrix} = R_g \begin{bmatrix} i_{ga} \\ i_{gb} \\ i_{gc} \end{bmatrix} + L_g \frac{d}{dt} \begin{bmatrix} i_{ga} \\ i_{gb} \\ i_{gc} \end{bmatrix} + \begin{bmatrix} V_{gca} \\ V_{gcb} \\ V_{gcc} \end{bmatrix} \quad (13)$$

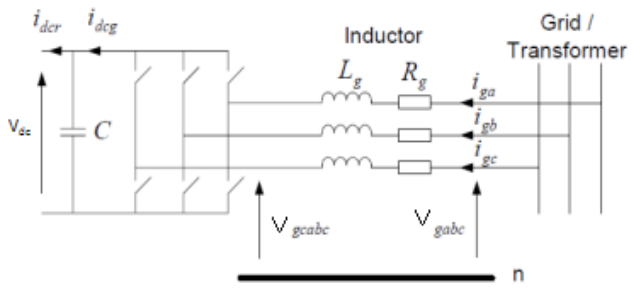

Figure 7. Grid-side PWM voltage source converter.

Using the abc-to-dq transformation matrix, the corresponding equation in the dq-reference frame, rotating at w_e is

$$V_{gd}=R_g i_{gd}+L_g\frac{di_{gd}}{dt}-\omega_e L_g i_{gq}+V_{gcd} \quad (14)$$

$$V_{gq}=R_g i_{gq}+L_g\frac{di_{gq}}{dt}+\omega_e L_g i_{gd}+V_{gcq} \quad (15)$$

The active (P_g) and reactive (Q_g) power flow between the grid and GSC can be given by[28].

$$P_g=\frac{3}{2}(V_{gd}i_{gd}+V_{gq}i_{gq}) \quad (16)$$

$$Q_g=\frac{3}{2}(V_{gq}i_{gd}-V_{gq}i_{gq}) \quad (17)$$

The angular position θ_e of grid voltage is calculated as

$$\theta_e=\int\omega_e dt=\tan^{-1}\left(\frac{V_{g\beta}}{V_{g\alpha}}\right) \quad (18)$$

where $V_{g\alpha}$ and $V_{g\beta}$ are the stationary dq-axis grid voltage components.

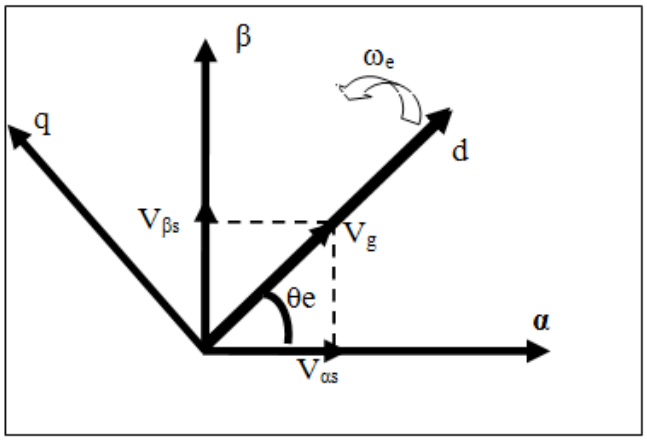

Figure 8. Vector diagram for GSC control.

By aligning d-axis of reference frame along grid voltage position, expressed by (18) and shown in Figure 8, V_{gq} is made zero which results V_{gd} equal to the amplitude of the grid voltage, a constant. Under such circumstances, from (16) & (17), the active and reactive power flow between the grid and GSC become proportional to i_{gd} and i_{gq} respectively. Figure 9 shows the vector control scheme employed for grid side PWM voltage control converter.

$$P_g=\frac{3}{2}V_{gd}i_{gd} \quad (19)$$

$$Q_g=-\frac{3}{2}V_{gd}i_{gq} \quad (20)$$

3.2 Vector-control Scheme of RSC

The RSC of DFIG is controlled in synchronously rotating dq-axis frame, with d-axis oriented along stator-flux vector position, shown in Figure 10. The PWM voltage source converter is current regulated with the d-axis current used to regulate the stator reactive power and q-axis current used to regulate the stator active power.

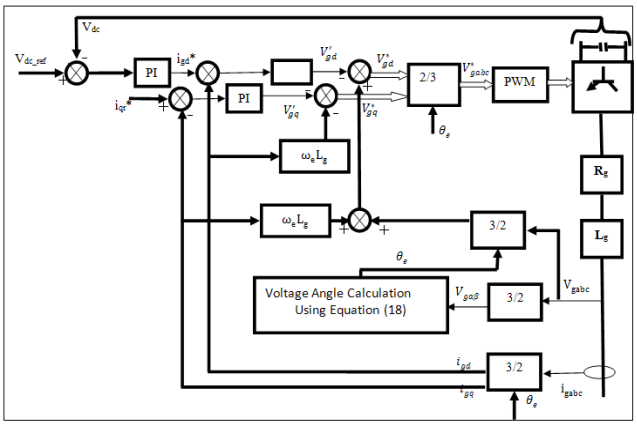

Figure 9. Vector-Control of GSC.

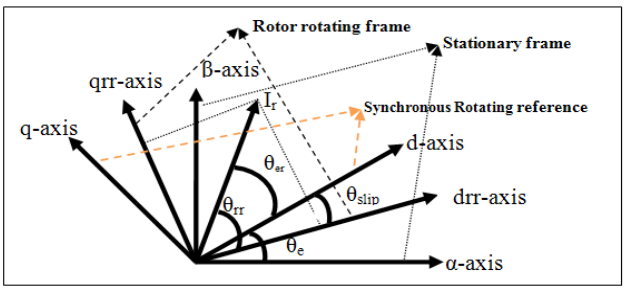

Figure 10. Vector diagram for RSC control.

The stator fluxes and the unit vectors for field orientation is computed as

$$\Psi_{\alpha s}=\int(V_{\alpha s}-R_s i_{\alpha s})dt;\psi_{\beta s}=\int(V_{\beta s}-R_s i_{\beta s})dt \quad (21)$$

$$\psi_s=\sqrt{(\psi_{\alpha s})^2+\left(\psi_{\beta s}\right)^2};\sin(\theta_e)=\frac{\psi_{\beta s}}{\psi_s};\cos(\theta_e)=\frac{\psi_{\alpha s}}{\psi_s} \quad (22)$$

Aligning the d-axis of the reference frame along stator-flux vector position, shown in Figure 10, ψ_{qs} is made zero which results the DFIG model[28] as:

$$\left.\begin{aligned}
&V_{sd}=0;V_s=V_{sq}=\omega_s\psi_{sd}\\
&V_{rd}=R_r i_{rd}+\sigma L_r\frac{di_{rd}}{dt}-\omega_{slip}\sigma L_r i_{rq}\\
&V_{rq}=R_r i_{rq}+\sigma L_r\frac{di_{rq}}{dt}+\omega_{slip}(L_{mm}i_{ms}+\sigma L_r i_{rd})\\
&\psi_s=\psi_{sd}=L_m i_{ms}=L_s i_{sd}+L_m i_{rd}\\
&0=L_s i_{sq}+L_m i_{rq},\psi_{rd}=\frac{L_m^2}{L_s}i_{ms}+\sigma L_r i_{rd}\\
&\psi_{rq}=\sigma L_r i_{rq}
\end{aligned}\right\} \quad (23)$$

where,

$$\omega_s=\omega_e;\omega_{slip}=\omega_s-\omega_r;\sigma=1-\frac{L_m^2}{L_s L_r}\text{ and }L_{mm}=\frac{L_m^2}{L_s}$$

The dq-axis rotor currents (i_{rd} and i_{rq}) in the synchronously rotating reference frame are given by

$$i_{rq}=-\frac{L_s}{L_m}i_{sq} \quad (24)$$

$$i_{rd}=\frac{\psi_{sd}-L_s i_{sd}}{L_m} \quad (25)$$

Rotor current vector magnitude ($|I_r|$) and its angle with respect to the rotor reference frame are[19],

$$|I_r|=\sqrt{(i_{rrd})^2+(i_{rrq})^2} \quad (26)$$

$$\sin(\theta_{rr})=\frac{i_{rrq}}{|I_r|};\cos(\theta_{rr})=\frac{i_{rrd}}{|I_r|} \quad (27)$$

The angle of the rotor current frame with respect to the d-axis of the stator flux oriented reference (θ_{er}) is computed from

$$\sin(\theta_{er})=\frac{i_{rq}}{|I_r|};\cos(\theta_{er})=\frac{i_{rd}}{|I_r|} \quad (28)$$

The stator-side active P_s and reactive Q_s power flow components become

$$P_s=-\frac{3}{2}\left(\frac{L_m}{L_s}V_s i_{rq}\right) \quad (29)$$

$$Q_s=\frac{3}{2}V_s\left(\frac{V_s}{\omega_s L_s}-\frac{L_m}{L_s}i_{rd}\right) \quad (30)$$

For constant stator voltage, Vs the stator-side active and reactive powers are directly proportional to i_{rq} and i_{rd} respectively. Figure 11 shows the proposed speed sensorless vector-control scheme for PWM rotor side voltage source converter and dotted blocks are new contributions of this paper.

4. Slip Speed Estimation

A new PLL is designed to define the reference angle for dq transformation so that the rotor current can be aligned along the q-axis and is included in the overall model of the system to make the designed system more realistic. Figure 12 shows the 3-phase PLL which takes the input as the measured DFIG rotor current and transforms it to dq-reference frame. PLL aligns the rotor side current to q-axis by comparing d-axis rotor current with zero reference current. The current error signal is passed through the PI controller to obtain the slip angular frequency of the rotor current. Hence in the PLL system:

$$I_{rd}=-I_r^*\sin(\theta_i-\theta_{slip})=>0=-I_r^*\sin(\theta_i-\theta_{slip})=>\theta_i=\theta_{slip} \quad (31)$$

Now the error signal is given as $e=0-i_{rd}=i_r\sin(\theta_i-\theta_{slip})$.

If $(\theta_i-\theta_{slip})$ is very small, then we can write: $\sin(\theta_i-\theta_{slip}) \approx (\theta_i-\theta_{slip})$. From the block diagram shown in Figure 12, $I_r(\theta_i-\theta_{slip})$ is the input to the controller and ω_{slip} is the output from the controller. Hence,

$$I_r\left(\theta_i-\theta_{slip}\right)K_{PLL}=\omega_{slip} \quad (32)$$

$$\frac{1}{I_r}\frac{d}{dt}\left(\theta_{slip}\right)=\left(\theta_i-\theta_{slip}\right)K_{PLL} \quad (33)$$

where,

$$K_{PLL}=K_p+\frac{K_I}{s}$$

5. Simulation Results and Discussion

The model of the complete system has been prepared using MATLAB/Simulink and simulations have been carried out for the complete model. All relevant parameters are

given in the Appendix. The time responses of Reference & actual speed (w_r), C_p (power Co-efficient), Speed slip (ω_{slip}), Reference & actual stator power (P_s), Reference & actual reactive power (Q_s), mechanical & electrical torque (T_m & T_e), dq-axis rotor currents (I_{rd}, I_{rq}), dq-axis stator voltage (V_{sd}, V_{sq}), Reference & actual DC-link voltage (V_{dc}), Rotor Power (P_r), single phase rotor current, dq-axis grid side converter current (I_{dg}, I_{qg}) and Grid Reactive power (Q_g), in response to the changes in the wind velocity {below, above and rated wind speed (=12m/s)}, are shown in Figures below.

5.1 Transient Response without Pitch Controller

5.1.1 For Wind Velocity Variations from below Rated to Rated and Back to Below Rated (i.e. 8m/s to 12m/s to 8m/s)

During 0 to 8 sec time interval wind velocity is 8 m/s (below the rated wind speed 12 m/s). In this time interval, simulation result shows that the rotor side active power controller adjust the turbine speed to make power coefficient maximum (approximately 0.48) as per the command of MPPT controller to capture maximum power (at zero pitch angle). As the generator operates below synchronous speed (i.e. sub-synchronous mode), the rotor absorbs active power from the grid (positive rotor power as shown in Figure 18).

During time interval 8 to 18 sec, a ramp increase in wind velocity from 8 m/s to 12 m/s at t = 8 sec. Controller adjusts the rotor speed to capture maximum active power output from the varied wind speed. Reactive power is regulated to a zero value for unity power factor generation. It is observed that when generator changes from sub-synchronous mode to super-synchronous mode of operation, the rotor delivers active power to the grid (Negative rotor power as shown in Figure 18). Also, Figure 19 shows the rotor current changes its phase while the operation changes from sub-synchronous to super-synchronous mode of operation and vice-versa. Although MPPT controller tracks the Cp maximum value corresponding to maximum power with respect to variation speed below the rated value 12 m/s, there is deviation in actual Cp value from Cp-max is observed during transient period. Hence, there is little deviation in the speed tracking and active power tracking response also observed before they track their respective reference values as shown in Figure 13 (a)-(d) and Figure 14 (a).

During time interval 18 to 25 sec, a ramp decrease in wind velocity from 12 m/s to 8 m/s at t = 18 sec. The rotor speed is again adjusted by the controller to capture maximum active power from the wind as like in the first interval. From Figure 13(b), Figure 14(a)-(c) and Figure 15(a)-(b), it is also observed that the change in the stator active power generated, rotor speed and electromagnetic torque corresponding to the variation in the wind speed is due to change in the rotor q-axis current by the active power PI controller; Similarly, the reactive power PI controller controls the d-axis rotor current to be at zero value (approximately) so as to generate zero reactive power for unity power factor power generation at constant stator (Grid) voltage (constant V_{qs} with V_{ds}=0 as shown in Figure 17(i)-(j)) level. Figure 17, Figure 20, Figure 21, Figure 22 and Figure 23 shows the V_{dc} link voltage remains almost constant throughout the operation by controlling the d-axis gird side converter current through dc-link voltage PI controller of GSC while the reactive power fed to grid is zero value by controlling the q-axis grid side converter current to zero value to maintain unity displacement factor.

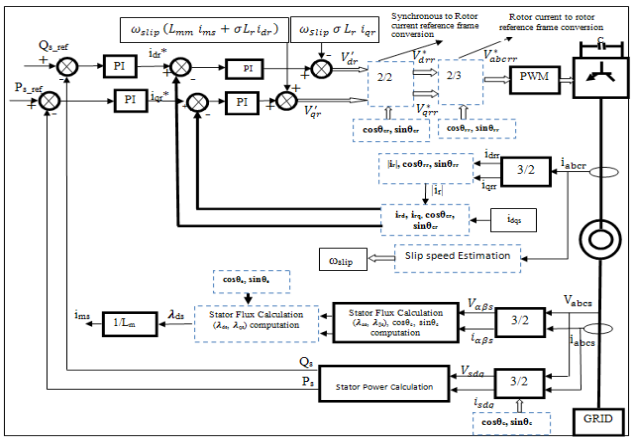

Figure 11. Speed Sensor-less Vector-control structures for RSC.

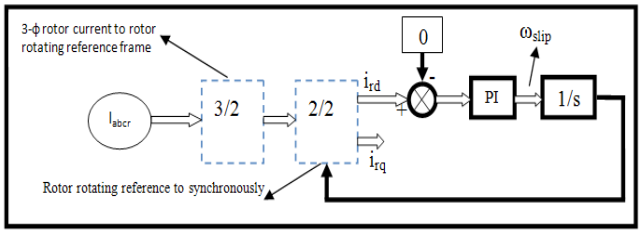

Figure 12. PLL based Slip speed estimator.

5.2 Transient Response with Pitch Controller

5.2.1 *For Wind Speed Variations from Below Rated to Above Rated and Back to Below Rated (i.e. 8m/s to 14m/s to 8m/s)*

In this case, with the ramp increase in wind velocity from 8 m/s to 14 m/s (above rated speed = 12 m/s) at t = 6 sec, it is observed that the pitch angle controller restricts the output power at rated power level by reducing the power co-efficient (corresponding to P_{max} value) with the increase in the blade pitch angle beta (β) as the wind speed increases above rated value 12 m/s as shown in Figure 24 (a)-(d). Accordingly β increases from zero value when wind speed increases above 12 m/s (between 6 to 7 sec) and reaches a value 5° approximately corresponding to reduced $C_{p\text{-}max}$ (3.2 approximate) at 14 m/s. It is also observed from Figure 24 (e)-(g) that active power PI controller changes the generated (stator) power as per the command of MPPT controller below the rated wind velocity and Pitch-angle controller above the rated wind speed with corresponding change in rotor speed and electromagnetic torque; similarly, reactive power PI-controller ensures zero stator reactive power for unity power factor generation. From Figure 24 (h)-(i), it can also be observed that the dc-link voltages PI-controller along with dq-axes current PI-controllers of GSC control the rotor power flow between GSC and Grid to maintain dc-link voltage almost constant under varying wind speed.

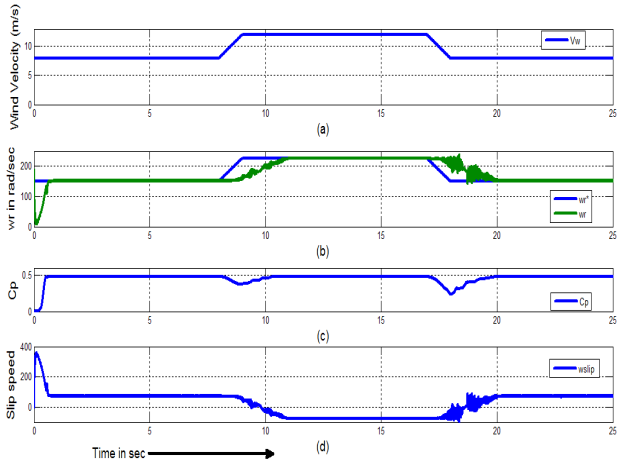

Figure 13. (a) Wind Velocity (b) Reference & actual generator speed (w_{r*} & w_r) (c) C_{pmax} and (d) Slip Speed. (ω_{slip}).

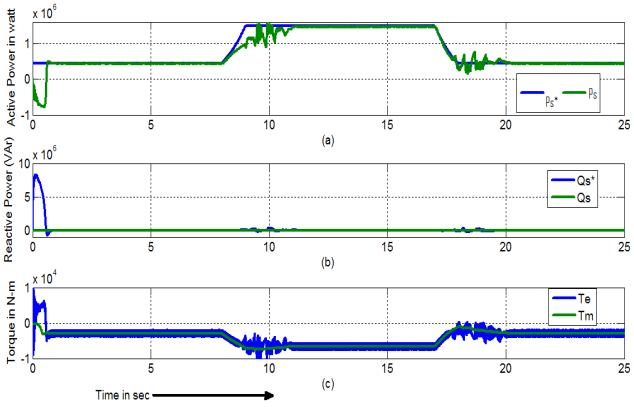

Figure 14. (a) Reference & Actual active power (P_{s*}, P_s), (b) Reference & Actual reactive power (Q_{s*}, Q_s) , (c) T_m & T_e (N-m).

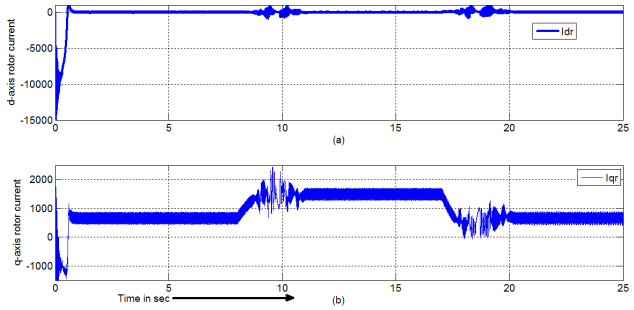

Figure 15. (a) d-axis rotor current (I_{rd}) & (b) q-axis current (I_{rq}).

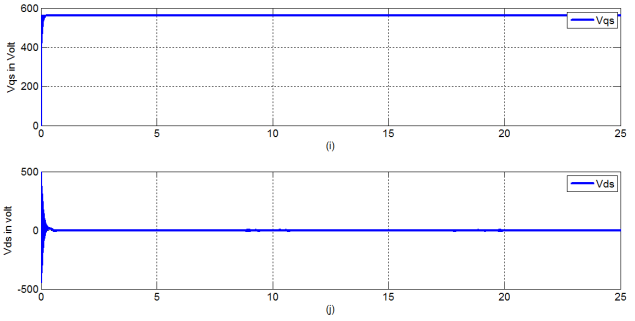

Figure 16. (i) q-axis stator voltage (V_{sq}) & (j) d-axis stator voltage (V_{sd}).

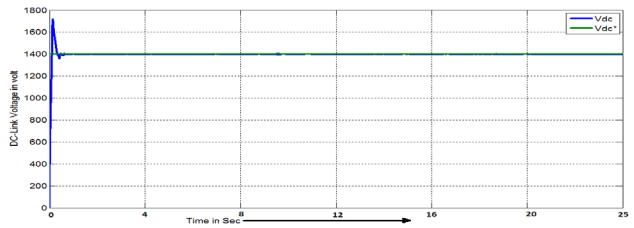

Figure 17. DC-link Voltage in volt.

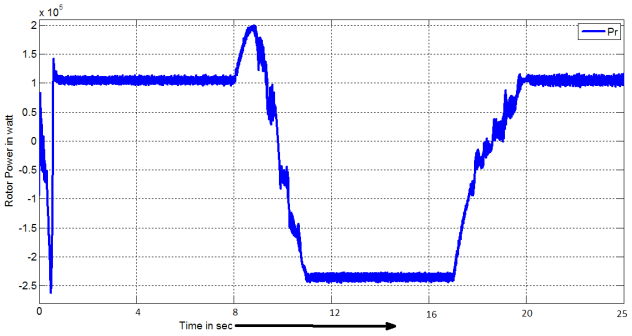

Figure 18. Rotor Power (P_r).

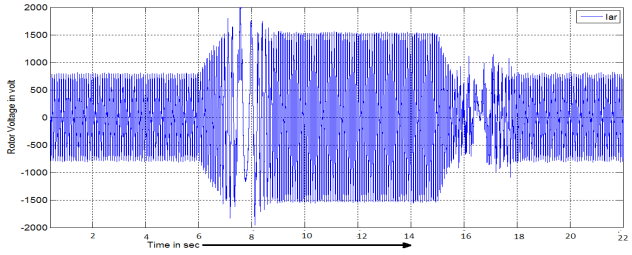

Figure 19. Single phase rotor current.

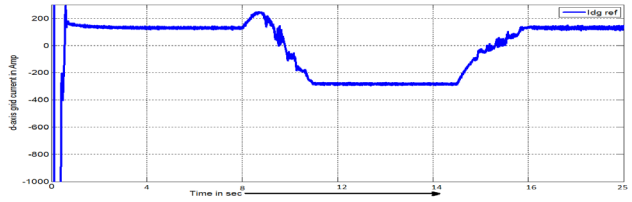

Figure 20. Reference d-axis grid side converter current.

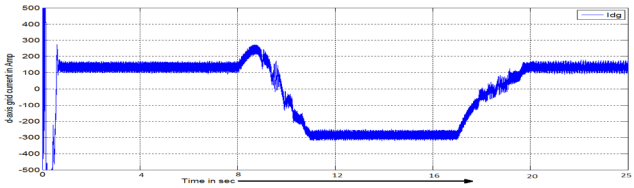

Figure 21. d-axis grid side converter current.

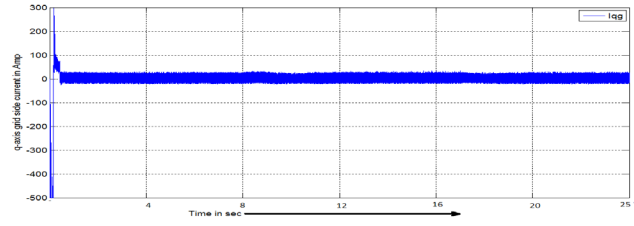

Figure 22. q-axis grid side converter current.

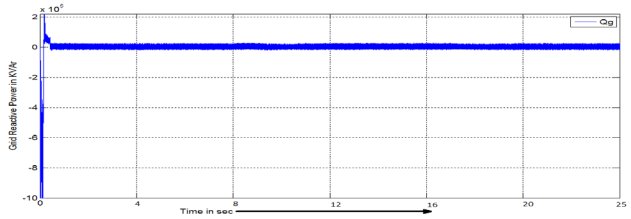

Figure 23. Grid Reactive power (Q_g).

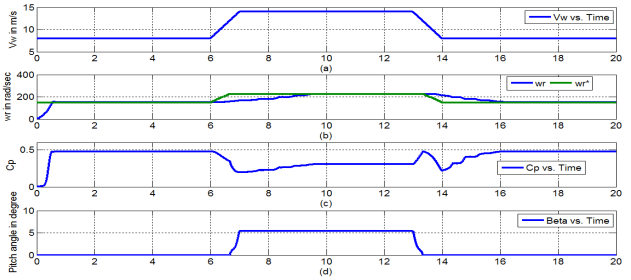

Figure 24. (a) wind velocity (V_w) (b) Reference & actual generator speed (w_{r^*} and w_r) (c) C_p and (d) Beta (pitch angle).

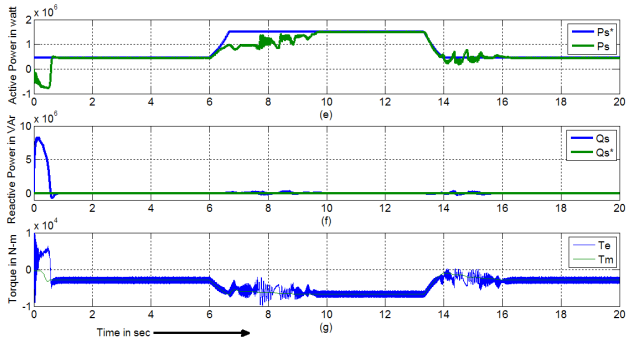

Figure 24. (e) Reference & actual stator power (Ps* & Ps in watt), (f) Reference & actual reactive power (Qs*& Qs in watt) and (g) Mechanical & Electromechanical torque (Tm & Te in N-m).

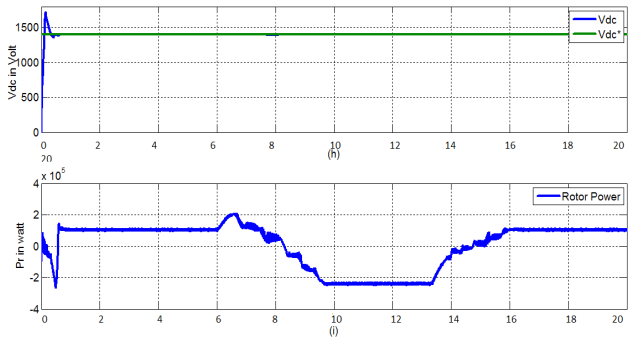

Figure 24. (h) Rotor Power (P_r) in watt & (i) DC-Link Voltage in volt.

6. Conclusion

This paper has investigated the performance of a 1.5MW DFIG based variable speed wind energy conversion system in MATLAB/Simulink environment. A PLL based slip speed estimator using three phase rotor current is proposed for speed sensor-less vector control operation of RSC to ensure decoupled control of stator active and reactive power while maximising the power generation at unity power factor under varying wind speed. Unlike previously reported methods the proposed speed sensor-less control algorithm used a PLL based slip speed estimator instead of rotor position or speed information for the stator field orientation of the rotor variables. This paper has also incorporated an optimal speed tracking controller mechanism and pitch angle controller mechanism for maximum energy capture during below the rated wind velocity and restricting the mechanical output power to its rated value during higher wind velocity respectively. The simulation result shows good dynamic response of Speed sensor-less DFIG based WECS under varying wind speed power generation.

7. References

1. Chowdhury BH, Chellapilla S. Double–Fed Induction Generator Control for Variable Speed Wind Power Generation. Elsevier Power System Research. 2006 Jun; 76(9–10):786–800.
2. Holdsworth L, Wu XG, Ekanayake JB, Jenkins N. Comparison of fixed speed and doubly-fed induction wind turbines during power system disturbances. IEE Proceeding General Transmit Distribute. 2003 May; 150(3):343–52.
3. Li G, Yin M, Zhou M, Zhao C. Decoupling control for multi terminal VSC HVDC based wind farm interconnection. IEEE Power Engineering Society General Meeting; 2007 Jun. p. 1–6.
4. Almeida RG, Castronuovo ED, Pacas Lopes JA. Optimum Control in Wind Parks when carrying out system Operator Requests. IEEE Transactions Power System. 2006 May; 21(2):718–25.
5. Nunes MVA, Zurn HH, Bezerra UH, Pecas Lopes JA, Almeida RG. Influence of the variable Speed wind Generators in Transient Stability Margin of the Conventional Generators Integrated in Electrical Grids. IEEE Transactions on Energy Conversion. 2004 Dec; 19(4):692–701.
6. Lei Y, Mullane A, Lightbody G, Yacamini R. Modeling of the wind turbine with a doubly fed Induction Generator for Grid Integration Studies. IEEE Transactions on Energy Conversion. 2006 Feb; 21(1):257–64.
7. Abolhassani M, Niazi P, Toliyat H, Enjeti P. A sensor-less integrated doubly-fed electric alternator/active filter (IDEA) for variable speed wind energy system. Proceedings 38th IAS Annual Meeting; 2003 Oct; 1:507–14.
8. Datta R, Ranganathan VT. A simple position sensor-less algorithm for rotor side field oriented control of wound rotor induction machine. IEEE Transactions Industrial. Electronics. 2001 Aug; 48(4):786–93.
9. Morel L, Godfroid H, Mirzaian A, Kauffmann JM. Double-fed induction machine: Converter optimization and field oriented control without position sensor. Proceeding Institute of Electrical and Electronics Engineers. 1998 Jul; 145(4):360–8.
10. Hopfensperger B, Atkinson DJ, Lakin RA. Stator-flux oriented control of a doubly-fed induction machine without position encoder. Proceeding Institute of Electrical and Ele ctronics Engineers. 2000 Jul; 147(4):241–50.
11. Mohammed OA, Liu Z, Liu S. A novel sensor-less control strategy of doubly fed induction motor and its examination with the physical modelling of machines. IEEE Transactions on Magnetics. 2005 May; 41(3):1852–55.
12. Mohammed OA, Liu Z, Liu S. A novel sensor-less control strategy of doubly-fed induction machines. Proceeding IEEE International Conference Electrical Mach Drives; 2005 May. p. 315–9.
13. Xu L, Cheng W. Torque and reactive power control of a doubly-fed induction machine by position sensor-less scheme. IEEE Transactions Industrial Applications. 1995 May/Jun; 31(3):636–41.
14. Carmeli S, Dezza FC, Perini R. Double fed induction machine drive: Proposal of a speed sensor-less control based on a MRAS. Proceeding IEEE International Conference Electrical Mach Drives; 2005 May. p. 404–10.
15. Schauder C. Adaptive speed identification for vector control of induction motors without rotational transducers. IEEE Transactions on Industrial Applications. 1992 Oct; 28(5):1054–61.
16. Kojabadi HM, Chang L, Doraiswami R. A MRAS-based adaptive pseudo reduced-order flux observer for sensor-less induction motor drives. IEEE Transactions on Power Electronics. 2005 Jul; 20(4):930–8.
17. Cardenas R, Pena R, Proboste J, Asher G, Clare J. MRAS observer for sensor-less control of stand-alone doubly-fed induction generators. IEEE Transactions on Energy Conversion. 2005 Dec; 20(4):710–8.
18. Cardenas R, Pena R, Clare J, Asher G, Proboste J. MRAS Observers for Sensor-less Control of Doubly-Fed Induction Generators. IEEE Transactions on Power Electronics. 2008 May; 23(3):1075–84.
19. Pattnaik M, Kastha D. Adaptive speed observer for stand-alone Doubly Fed Induction Generator feeding nonlinear and unbalanced loads. IEEE Transactions on energy conversion. 2012 Dec; 27(4):1018–26.

20. Qu L, Qiao W. Constant Power Control of DFIG Wind Turbines with Super capacitor Energy Storage. IEEE Transactions on Industrial Applications. 2011 Jan; 47(1):359–67.
21. Pokharel B. Modeling, Control and Analysis of a Doubly Fed Induction Generator Based Wind Turbine System with Voltage Regulation [MS Thesis]. Department of Electrical Engineering, Tennessee Technological University; 2011. p. 338.
22. Miller NM, Price WW, Sanchez-Gasca JJ. Dynamic Modeling of GE 1.5 and 3.6 Wind Turbine-Generators. GE-Power Systems Energy Consulting, General Electric International, Inc; 2003. p. 2.1–2.7.
23. Muhando EB, Senjyu T, Uehara A, Funabashi T, Kim C-H. LQG Design for Megawatt-Class WECS with DFIG Based on Functional Models' Fidelity Prerequisites. IEEE Transaction on Energy Conversion. 2009 Nov; 24(4):893–904.
24. Das MK, Chowdhury S, Chowdhury SP, Gaunt CT. Control of a Grid Connected Doubly-Fed Induction Generators for Wind Energy Conversion. Glasgow: Universities Power Engineering Conference; 2009 Sep. p. 1–5.
25. Krause PC, Wasynczuk O, Sudhoff SD. Analysis of Electric Machinery and Drive Systems. New Jersey: IEEE Press, Wiley-Interscience, John Wiley & Sons, Inc; 2013.
26. Pena R, Clear JC, Asher GM. Doubly fed induction generator using back-to-back PWM Converters and its application to variable-speed wind energy generation. IEE Proceedings-Elect Power Appl. 1996; 143(3):231–41.
27. Abraham1 A, Subramanian DP. Impact of parameter variations on the steady state behavior of grid connected renewable energy conversion systems. Indian Journal of Science and Technology. 2014 Oct; 7(S6):48–55.
28. Sun T. Power Quality of Grid-Connected Wind Turbines with DFIG and Their Interaction with the Grid [PhD Thesis]. Denmark: Institute of Energy Technology, Aalborg University; 2004 May.
29. Belmokhtar K, Doumbia ML, Agbossou K. Modelling and fuzzy logic control of DFIG based Wind Energy Conversion Systems. IEEE International Symposium on Industrial Electronics: Hangzhou. 2012 May. p. 1888–93.

8. Appendix

A. Specifications of Doubly fed Induction Generator[21]

Rated Capacity = 1.5MW; Optimal (Rated); Rotor speed=2158 rpm (Electrical); Wm (rated) =225.9 rad/sec (Mech.); No. of poles=4; Frequency=60 Hz; Ns (synchronous speed) = 1800 rmp; Rated Voltage (Line to line) = 690 V; Synchronous angular speed (Ws)= 188.5 rad/sec (Mech.); Shaft Inertia=18.7 kg.m^2; Lm=2.88mH; Rotor referred inductance=2.97mH; Ls=2.93 mH; Rotor referred resistance=2 m-ohm; R=2.3 m-ohm

B. Specifications of Wind turbine[21]:

Blade Radius=30.66m; Cut-in/cut-out wind speed=4/25 m/s; Gear Box=71.28; Rated wind speed=12 m/s; Air density=1.225 kg/m^3

C. Specification of converter[21]

DC-link Voltage=1400V; DC-link capacitor=60mF; Switching frequency=5000 Hz; Sampling time=2e-5; Lg =2mH; Rg =2mΩ.

Nomenclature

V_{gabc} = Three phase grid voltages [V]
V_{gcabc} = Three phase grid-side converter voltages [V]
I_{abcr} = Three phase rotor current [A]
i_{ga}, i_{gb}, i_{gc} = Three phase grid-side converter currents [A]
R_g and L_g = Resistance [Ω] and inductance [H] of grid side filter
i_{dcg} ,i_{dcr} = Grid-side and rotor-side DC currents [A]
C = DC-link capacitor [F]
V_{gcd} & V_{gcq}=grid side converter voltage in d & q axis
i_{gd} & i_{gq}=grid side converter current in d & q axis
ω_e = Rotational speed of the grid voltage (elec. Rad/sec)
$\psi_{\alpha s}$, $\psi_{\beta s}$ = Stationary αβ -axis stator fluxes [Wb]
$V_{\alpha s}$,$V_{\beta s}$ = Stationary αβ-axis stator voltages [V]
$i_{\alpha s}$ $i_{\beta s}$ = Stationary αβ-axis stator currents [A]
ω_s = Electrical angular velocity of the stator flux [rad/s]
V_s =Magnitude of the stator phase voltage [V]
V_{gd} & V_{gq}=Gird dq- axis voltages
ψ_s=Magnitude of the stator flux linkage [Wb]
i_{ms} =Magnetising current [A] of the generator
V_{abcrr*} = Reference values of the 3-Φ rotor voltages [V]
V_{drr*}, V_{qrr*} = Rotor dq-axies reference voltages [V]
i_{dr*}, i_{qr*} = Rotor d- and q-axis reference currents [A]
ω_r = Generator speed (rad/s)
ω_t =Blade turbine speed (rad/s)
T_m= Mechanical Torque (N-m)
P_{rated}= Rated power (watt)
R = Blade radius of the wind turbine (m)
V_w = Wind speed at the centre of the rotor blade (m/sec)
ρ = Air density (Kg/m^3)
A = Blade swept area of the wind turbine (m^2)

E_w = Kinetic energy of wind
C_p = Power coefficient of wind turbine
$\boldsymbol{\lambda}$=Tip Speed Ratio
β = Pitch angle
θ_{er}= Angle between synchronously rotating reference frame and rotor current reference frame.
θ_{rr}= Angle between rotor rotating reference frame and rotor current reference frame.
θ_{slip}= Angle between synchronously rotating reference frame and rotor rotating reference frame.